GSM-Based Non-Orthogonal Multiple Access: Design and Evaluation

Surjeet Kumar*, Ashish Kant Shukla†, Manav R. Bhatnagar*
*Department of Electrical Engineering, Indian Institute of Technology Delhi, New Delhi 110016, India
†Department of Electronics and Communication Engineering, SR University, Warangal, Telangana 506371, India
*{surjeet.kumar, manav}@ee.iitd.ac.in, †ashish@sru.edu.in

***Abstract*—This paper proposes a novel generalized spatial modulation non-orthogonal multiple access (GSM-NOMA) framework to enhance symbol transmission and active antenna index detection in a two-user scenario. The system employs space-domain NOMA and accounts for practical limitations by incorporating imperfect successive interference cancellation (SIC) at the near user. Key contributions include robust decoder design, closed-form average bit error rate expressions (ABER) capturing symbol and index errors, and an optimized power allocation strategy. Simulation results validate the proposed approach, demonstrating notable improvements in spectral efficiency, reliability, and robustness, making GSM-NOMA a promising solution for next-generation wireless communication systems.**

***Index Terms*—Generalized spatial modulation (GSM), non-orthogonal multiple access (NOMA), optimal power allocation, space-domain NOMA, successive interference cancellation (SIC).**

I. Introduction

Future wireless networks must meet strict requirements such as ultra-high data rates, low latency, massive connectivity, and high energy efficiency [1]–[3]. Non-orthogonal multiple access (NOMA) has emerged as a key solution, enabling multiple users to share the same time-frequency resources via power-domain multiplexing, thereby boosting spectral efficiency [4]. By using superposition coding (SC) at the transmitter and successive interference cancellation (SIC) at the receiver, NOMA supports dense user deployments and is regarded as a key enabler for next-generation wireless standards [5], [6].

Meanwhile, spatial-domain techniques such as spatial modulation (SM) [7] are advancing rapidly. SM encodes part of the information using the index of a single active transmit antenna, improving spectral efficiency while reducing interference. However, relying on a single active antenna limits system diversity and reliability. Generalized spatial modulation (GSM) addresses this by activating multiple antennas, encoding more bits in the antenna pattern, and providing both higher spectral efficiency and spatial diversity [8].

While GSM improves reliability and retains the low-complexity detection advantage of SM, it requires precise antenna synchronization to avoid inter-symbol interference. Although NOMA and GSM have received significant research attention, most studies have treated them separately or explored them in limited hybrid forms. NOMA research has focused on enhancing performance through advanced precoding, artificial noise (AN) for security, and integration with millimeter-wave (mmWave) communications [9]. GSM research has concentrated on optimizing antenna activation patterns, reducing complexity, and ensuring compatibility with emerging access schemes [10], [11]. Hybrid schemes such as variable active spatial modulation (VASM) with NOMA [11] and NOMA-GSM using transmit antenna combinations [10] have shown potential. GSM-based methods have also been integrated into large-scale access frameworks [12]. Despite these advancements, the application of space-domain NOMA principles to GSM-based active antenna index transmission remains largely unexplored, presenting a significant research gap.

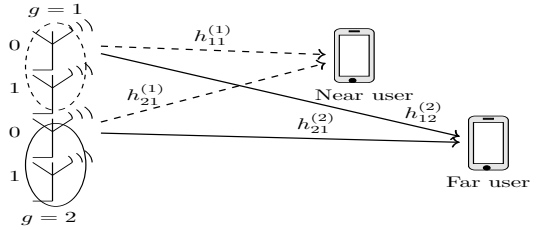

Fig. 1. System model.

To address this gap, we propose a novel GSM-NOMA framework that combines the spatial diversity of GSM with the spectral efficiency of NOMA.

Our main contributions are as follows:

- We propose a GSM-NOMA scheme that utilizes power-domain multiplexing across multiple active antennas, improving both spatial indexing and symbol transmission in a two-user setup.
- We design decoding strategies for both users, enabling efficient recovery of the transmitted symbols and antenna activation patterns within the constraints of NOMA.
- Closed-form expressions are derived for the average bit error rate (ABER) related to both symbol and active antenna index errors, offering analytical insights into the system's performance.
- An optimized power allocation strategy is introduced–based on the derived ABER expressions enhancing the overall performance of the system.

II. System Model

Consider a two-user downlink NOMA scenario, as shown in Fig. 1. A base station (BS) with $N_t = 4$ transmit antennas serves a near user and a far user. The antennas are grouped into two sets, each with binary indices. For each user, one group maps binary digits 0 and 1 to different antennas, allowing the BS to encode information in the spatial domain using GSM.

From the first group of antennas ($g = 1$), one antenna is activated to represent bits 0 or 1 for the near user, and from the second group ($g = 2$), another antenna is activated for the far user. During each transmission, a total of $N_a = 2$ antennas are activated, one from each group, embedding spatial information for both users.

To implement NOMA, the BS uses SC to combine the near and far user signals. A power allocation factor $\alpha \in (0,1)$ is assigned to the near user, with the far user receiving $1-\alpha$. The signal is a superimposed mixture of both users' data on selected antennas, allowing them to share the same time-frequency resources.

The BS selects one active antenna from each group and assigns distinct power levels based on NOMA principles. The near user's channel is scaled by $\beta \in (0,1)$, and the far user's channel is scaled by $1-\beta$. SC is then used to transmit both users' signals and their active antenna indices over the same time-frequency resources.

The downlink channel from the BS to user k ($k=1$ for the near and $k=2$ for the far) via active antenna $a_g \in \{1,2\}$ is modelled by: $h_{g,a_g}^{(k)} = (d^{(k)})^{-\delta} h_w$, where $d^{(k)}$ denotes the BS user distance in meter, δ is the path-loss exponent, and $h_w \sim \mathcal{CN}(0,1)$ represents a complex Gaussian fading coefficient. The near user typically has a stronger channel, i.e., $|h_{g,a_g}^{(1)}|^2 > |h_{g,a_g}^{(2)}|^2$. The channel follows a flat-fading model, with perfect channel state information (CSI) assumed at the receiver. Additive white Gaussian noise (AWGN) with variance σ_n^2 is present at the receivers.

A. GSM-Based NOMA Transmission

Let $x^{(k)}$ denote the unitary binary phase shift keying (BPSK) constellation symbols intended for transmission to user k. Following the principles of NOMA, the symbols $x^{(1)}$ and $x^{(2)}$ are superimposed as:

$$z = \sqrt{\alpha}\, x^{(1)} + \sqrt{1-\alpha}\, x^{(2)}, \tag{1}$$

where $\mathbb{E}[zz^*] = 1$(where $\mathbb{E}[\cdot]$ denotes the expectation) ensures normalized transmit power. The BS employs a single active antenna from each group, applying the NOMA scheme on the selected antennas. The aggregated channel coefficients for the active antennas are denoted as $h_{1,a_1}^{(k)}$ for the first group and $h_{2,a_2}^{(k)}$ for the second group. These coefficients represent the SC active antenna channels for near or far user transmission and are modeled as:

$$h_t^{(k)} = \sqrt{\beta}\, h_{1,a_1}^{(k)} + \sqrt{1-\beta}\, h_{2,a_2}^{(k)}, \tag{2}$$

where $h_t^{(k)}$ corresponds to the SC active antenna channel coefficients, with the subscript t taking values from $\{1,2,3,4\}$ to represent combinations of group indices g and active antenna indices a_g. This results in four unique coefficients, as detailed in Table I. Finally, the received NOMA signals for the near and far users are given by:

$$y_t^{(k)} = h_t^{(k)} z + e_t^{(k)}, \tag{3}$$

where $e_t^{(k)}$ represents AWGN.

B. Decoder Design and Active Antenna Estimation

This subsection details the decoder design for the proposed GSM-NOMA framework, which enables symbol detection for both near and far users while incorporating active antenna (or index) estimation. The general decoding process is depicted in Fig. 2. Specifically, Fig. 2(a) illustrates the symbol decoding process for near and far users, assuming prior knowledge of the active antenna a_g within group g. On the other hand, Fig. 2(b) demonstrates the active antenna estimation mechanism, where the receiver is assumed to have prior knowledge of the transmitted symbol.

TABLE I: GSM Mapping Table for $N_t = 4$ and $N_a = 2$

Grouped Bits	Antenna Combination (g, a_g)	t	SC Active Antenna Channel Coefficient h_t
[0 0]	$(1,1),(2,1)$	1	$\sqrt{\beta}h_{1,1}^{(k)} + \sqrt{1-\beta}h_{2,1}^{(k)}$
[0 1]	$(1,1),(2,2)$	2	$\sqrt{\beta}h_{1,1}^{(k)} + \sqrt{1-\beta}h_{2,2}^{(k)}$
[1 0]	$(1,2),(2,1)$	3	$\sqrt{\beta}h_{1,2}^{(k)} + \sqrt{1-\beta}h_{2,1}^{(k)}$
[1 1]	$(1,2),(2,2)$	4	$\sqrt{\beta}h_{1,2}^{(k)} + \sqrt{1-\beta}h_{2,2}^{(k)}$

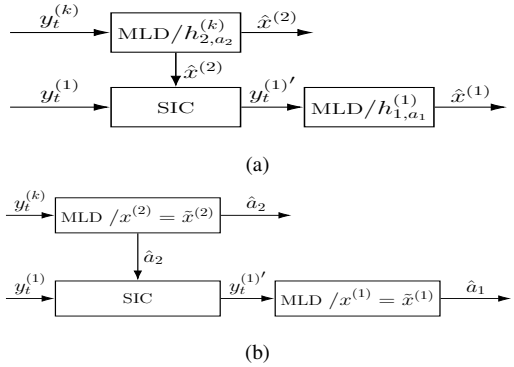

Fig. 2. (a) Symbol decoding process (b) Active antenna estimation.

At the far user's symbol, $x^{(2)}$, the maximum-likelihood detector (MLD) is formulated as:

$$\hat{x}^{(2)} = \min_{\tilde{x}^{(2)} \in \mathcal{X}^{(2)}} \left| y_t^{(2)} - \sqrt{(1-\alpha)(1-\beta)} h_{2,a_2}^{(2)} \tilde{x}^{(2)} \right|^2, \tag{4}$$

where $\mathcal{X}^{(2)} = \{-1, 1\}$ represents the BPSK constellation. Once the transmitted symbol $x^{(2)}$ is known at the receiver, the active antenna for the far user can be estimated using MLD as follows:

$$\hat{a}_2 = \min_{\tilde{a}_2 \in \{1,2\}} \left| y_t^{(2)} - \sqrt{(1-\alpha)(1-\beta)} h_{2,\tilde{a}_2}^{(2)} x^{(2)} \right|^2, \tag{5}$$

where $\tilde{a}_2$ represents the index of the far user's active antenna.

After detecting the far user's symbol, the near user initially treats its symbol as noise. It decodes $x^{(2)}$ and the active antenna a_2 using (4) and (5), with the superscripts of the received signal and channel gain updated from 2 to 1. To mitigate interference, SIC is employed to remove the contribution of the far user from the received signal:

$$y_t^{(1)'} = y_t^{(1)} - \sqrt{(1-\alpha)(1-\beta)} h_{2,\hat{a}_2}^{(1)} \hat{x}^{(2)}, \tag{6}$$

once interference is removed, the near user's symbol, $\hat{x}^{(1)}$, is estimated using MLD as follows:

$$\hat{x}^{(1)} = \min_{\tilde{x}^{(1)} \in \mathcal{X}^{(1)}} \left| y_t^{(1)'} - \sqrt{\beta\alpha} h_{1,a_1}^{(1)} \tilde{x}^{(1)} \right|^2, \tag{7}$$

where $\mathcal{X}^{(1)} = \{-1, 1\}$ denotes the BPSK constellation. Assuming $x^{(1)}$ is known at the receiver, the MLD-based active antenna estimation is:

$$\hat{a}_1 = \min_{\tilde{a}_1 \in \{1,2\}} \left| y_t^{(1)'} - \sqrt{\beta\alpha} h_{1,\tilde{a}_1}^{(1)} x^{(1)} \right|^2, \tag{8}$$

where $\tilde{a}_1$ denotes the near user's active antenna index.

III. Performance Analysis

This section presents the evaluation of the ABER and optimized power allocation for the proposed GSM-NOMA scheme to enhance system performance.

A. Error Probability for Far User Symbol Detection

The received signal for the far user is influenced by interference from the near user's transmission and the first group's active antenna. Due to the far user's weak channel conditions, SIC is not performed. From (3), the received signal for the far user can be expressed as:

$$y_t^{(2)} = \sqrt{\gamma^{(2)}}\, h_{2,a_2}^{(2)}\, x^{(2)} + \mathcal{I}^{(2)} + e_t^{(2)}, \tag{9}$$

where $\gamma^{(2)} = (1-\beta)(1-\alpha)$, and the total interference term $\mathcal{I}^{(2)}$ is given by:

$$\mathcal{I}^{(2)} = \sqrt{(1-\beta)\alpha}\, h_{2,a_2}^{(2)} x^{(1)} + \sqrt{\beta}\, h_{1,a_1}^{(2)} z, \tag{10}$$

where $\sqrt{(1-\beta)\alpha}\, h_{2,a_2}^{(2)} x^{(1)}$ accounts for interference from the near user's symbol, and $\sqrt{\beta}\, h_{1,a_1}^{(2)} z$ represents interference from the first group's active antenna. Substituting (9) and (10) into (4), the estimated far user symbol can be expressed as:

$$\hat{x}^{(2)} = \min_{\tilde{x}^{(2)} \in \mathcal{X}^{(2)}} |\sqrt{\gamma^{(2)}} h_{2,a_2}^{(2)} (x^{(2)} - \tilde{x}^{(2)}) + \mathcal{I}^{(2)} + e_t^{(2)}|^2, \tag{11}$$

where the active antenna coefficient $h_{2,a_2}^{(2)}$ is assumed to be known at the receiver. Using the findings from [13], the BER for the far user can be expressed as:

$$P_{e,\text{symbol}}^{(2)}(h_{2,a_2}^{(2)}) = Pr\left(w_1 < -|U_1|^2\right), \tag{12}$$

where $U_1 = \sqrt{\gamma^{(2)}} h_{2,a_2}^{(2)} 2x^{(2)} + \mathcal{I}^{(2)}$, and $w_1 = 2\Re\{U_1 (e_t^{(2)})^*\}$. Where $(\cdot)^*$ denotes the complex conjugate, and $\Re\{\cdot\}$ represents the real part. Since $w_1 \sim \mathcal{N}(0, 2|U_1|^2\sigma_n^2)$, using the cumulative distribution function (CDF) property: $Pr(w < b) = Q\left(\frac{-b}{\sigma_w}\right)$, $P_{e,\text{symbol}}^{(2)}$ is rewritten in terms of w_1's distribution:

$$P_{e,\text{symbol}}^{(2)}(h_{2,a_2}^{(2)}) = \mathrm{Q}\left(|U_1|/\sqrt{2}\sigma_n\right), \tag{13}$$

with $a = 1/\sqrt{2}\sigma_n$ and $\mathrm{Q}(\cdot)$ as the Q-function, $U_1 \sim \mathcal{CN}(0, \sigma_{u_1}^2)$ with $\sigma_{u_1}^2 = (\beta + (1-\beta)(4-3\alpha))\sigma_{h^{(2)}}^2$. Averaging (13) over the Rayleigh-distributed $|U_1|$ as in [13, Eq. (15)], the far user's ABER is:

$$P_{e,\text{symbol}}^{(2)} = (1/2) \times \left(1 - a/\sqrt{a^2 + 2/\sigma_{u_1}^2}\right). \tag{14}$$

Remark 1: At high signal-to-noise ratio (SNR), the expression simplifies as $1 - \frac{a}{\sqrt{a^2+2/\sigma_{u_1}^2}} \approx \frac{1}{a^2\sigma_{u_1}^2}$, yielding:

$$P_{e,\text{symbol}}^{(2)} \approx 1/2a^2\sigma_{u_1}^2. \tag{15}$$

B. Error Analysis for Far User Antenna Estimation

This section examines the error probability in detecting the active antenna for the second group assigned to the far user. The goal is to determine whether the active index is 0 or 1. Assuming the transmitted symbol $x^{(2)}$ is known at the receiver ($\tilde{x}^{(2)} = x^{(2)}$), using (5) the estimated active antenna index $\hat{a}_2$ is given by:

$$\hat{a}_2 = \min_{\tilde{a}_2 \in \{1,2\}} \left|\sqrt{\gamma^{(2)}}(h_{2,a_2}^{(2)} - h_{2,\tilde{a}_2}^{(2)}) + \mathcal{I}^{(2)} + e_t^{(2)}\right|^2, \tag{16}$$

evaluating (16) using (11) leads to the error probability:

$$P_{e,\text{index}}^{(2)}(h_{2,a_2}^{(2)}) = Pr\left(w_2 < -|U_2|^2\right), \tag{17}$$

where $U_2 = \sqrt{\gamma^{(2)}}\,(h_{2,a_2}^{(2)} - h_{2,\tilde{a}_2}^{(2)})x^{(2)} + \mathcal{I}^{(2)}$ and $w_2 = 2\Re\{U_2 (e_t^{(2)})^*\}$. The term w_2 follows a normal distribution with mean $\mu_{w_2} = 0$ and variance $\sigma_{w_2}^2 = 2|U_2|^2\sigma_n^2$, i.e., $w_2 \sim \mathcal{N}(\mu_{w_2}, \sigma_{w_2}^2)$. Solving (17) analogously to (12) yields:

$$P_{e,\text{index}}^{(2)}(h_{2,a_2}^{(2)}) = \mathrm{Q}\left(|U_2|/\sqrt{2}\sigma_n\right), \tag{18}$$

similarly, $U_2 \sim \mathcal{CN}(0, \sigma_{u_2}^2)$ with $\sigma_{u_2}^2 = (1 + \gamma^{(2)})\sigma_{h^{(2)}}^2$. Averaging (18) as in (13), the far user's average antenna index error probability is:

$$P_{e,\text{index}}^{(2)} = (1/2) \times \left(1 - a/\sqrt{a^2 + 2/\sigma_{u_2}^2}\right), \tag{19}$$

Remark 2: At high SNR, the average antenna index error probability for the far user simplifies to an approximation given by :

$$P_{e,\text{index}}^{(2)} \approx (1/2)a^2\sigma_{u_2}^2. \tag{20}$$

The overall BER $P_e^{(2)}$ includes errors from symbol estimation and active antenna index estimation, given by:

$$P_e^{(2)} = P_{e,\text{symbol}}^{(2)} + P_{e,\text{index}}^{(2)} - P_{e,\text{index}}^{(2)} P_{e,\text{symbol}}^{(2)}. \tag{21}$$

This accounts for the far user for both error types while correcting for their overlap.

C. Error Probability for Near User Symbol Detection

This section derives the ABER for the near user by analyzing the error probability of estimating its transmitted symbols. The received signal for the near user, $y_t^{(1)}$, as defined in (3), is expressed as:

$$y_t^{(1)} = \sqrt{\gamma^{(1)}}\, h_{1,a_1}^{(1)}\, x^{(1)} + \sqrt{\gamma^{(2)}}\, h_{2,a_2}^{(1)}\, x^{(2)} + \mathcal{I}^{(1)} + e_t^{(1)}, \tag{22}$$

where $\gamma^{(1)} = \beta\alpha$, and $\mathcal{I}^{(1)}$ represents the cumulative interference expressed as:

$$\mathcal{I}^{(1)} = \sqrt{\beta(1-\alpha)}\, h_{1,a_1}^{(1)}\, x^{(2)} + \sqrt{(1-\beta)\alpha}\, h_{2,a_2}^{(1)}\, x^{(1)}, \tag{23}$$

with $\sqrt{\beta(1-\alpha)} h_{1,a_1}^{(1)} x^{(2)}$ capturing interference from the far user's symbol, and $\sqrt{(1-\beta)\alpha}\, h_{2,a_2}^{(1)} x^{(1)}$ accounting for interference from the active antenna of the second group. By applying SIC to the near user's received signal, as described in (6), we obtain:

$$y_t^{(1)'} = \sqrt{\gamma^{(1)}}\, h_{1,a_1}^{(1)}\, x^{(1)} + \mathcal{I}_{SIC} + \mathcal{I}^{(1)} + e_t^{(1)}, \tag{24}$$

where $\mathcal{I}_{\text{SIC}}$ is the residual interference after SIC, defined as:

$$\mathcal{I}_{SIC} = \sqrt{\gamma^{(2)}}\,(\, h_{2,a_2}^{(1)} x^{(2)} - \, h_{2,\hat{a}_2}^{(1)} \hat{x}^{(2)}), \tag{25}$$

substituting (24) into (7) and performing algebraic simplifications, the near user's estimated symbol can be expressed as:

$$\hat{x}^{(1)} = \min_{\tilde{x}^{(1)} \in \mathcal{X}^{(1)}} \left|\sqrt{\gamma^{(1)}} h_{1,a_1}^{(1)} (x^{(1)} - \tilde{x}^{(1)}) + \mathcal{I}_{\text{SIC}} + \mathcal{I}^{(1)} + e_t^{(1)}\right|^2, \tag{26}$$

where (26) is solved according to (11). Thus, the symbol error probability for the near user is given by:

$$P^{(1)}_{e,\text{symbol}}(h^{(1)}_{1,a_1}) = \Pr\left(w_3 < -|U_3|^2\right), \tag{27}$$

where $U_3 = \sqrt{\gamma^{(1)}}\, h^{(1)}_{1,a_1}\, 2x^{(1)} + \mathcal{I}_{SIC} + \mathcal{I}^{(1)}$ and $w_3 = 2\Re\{U_3(e^{(1)}_t)^*\}$. Here, w_3 is characterized by a mean $\mu_{w_3} = 0$ and variance $\sigma^2_{w_3} = 2\,|U_3|^2\sigma^2_n$,i.e., $w_3 \sim \mathcal{N}(\mu_{w_3}, \sigma^2_{w_3})$. Solving (27) similarly to (12) yields:

$$P^{(1)}_{e,\text{symbol}}(h^{(1)}_{1,a_1}) = \mathrm{Q}\left(|U_3|/\sqrt{2}\sigma_n\right), \tag{28}$$

where $U_3 \sim \mathcal{CN}(0, \sigma^2_{u_3})$, with variance $\sigma^2_{u_3} = (\beta(1+3\alpha) + (1-\beta)(\alpha+(1-\alpha)\kappa))\sigma^2_{h^{(1)}}$. Where κ models SIC imperfection ($\kappa = 0$ for perfect SIC, $\kappa \in [0,1]$ for imperfections). Averaging (28), the near user's ABER is:

$$P^{(1)}_{e,\text{symbol}} = 0.5\left(1 - a/\sqrt{a^2 + 2/\sigma^2_{u_3}}\right). \tag{29}$$

Remark 3: At high SNR, the ABER for the near user can be approximated as:

$$P^{(1)}_{e,\text{symbol}} \approx 1/2a^2\sigma^2_{u_3}. \tag{30}$$

D. Error Analysis for Near User Antenna Estimation

This section analyzes the error probability in estimating the active antenna for the first group assigned to the near user. The objective is to determine whether the active antenna index is 0 or 1, assuming the transmitted symbol $x^{(1)}$ is known at the receiver ($\tilde{x}^{(1)} = x^{(1)}$). Based on (8), the estimated active antenna index $\hat{a}_1$ is given by:

$$\hat{a}_1 = \min_{\tilde{a}_1 \in \{1,2\}} \left|\sqrt{\gamma^{(1)}}(h^{(1)}_{1,a_1} - h^{(1)}_{1,\tilde{a}_1})x^{(1)} + \mathcal{I}_{SIC} + \mathcal{I}^{(1)} + e^{(1)}_t\right|^2, \tag{31}$$

where the expression in (31) is evaluated according to (11), resulting in:

$$P^{(1)}_{e,\text{index}}(h^{(1)}_{1,a_1}) = Pr\left(w_4 < -|U_4|^2\right), \tag{32}$$

where $U_4 = \sqrt{\gamma^{(1)}}(h^{(1)}_{1,a_1} - h^{(1)}_{1,\tilde{a}_1})x^{(1)} + \mathcal{I}_{SIC} + \mathcal{I}^{(1)}$ and $w_4 = 2\Re\{U_4(e^{(1)}_t)^*\}$. Here, w_4 is characterized by a mean $\mu_{w_4} = 0$ and variance $\sigma^2_{w_4} = 2|U_4|^2\sigma^2_n$,i.e., $w_4 \sim \mathcal{N}(\mu_{w_4}, \sigma^2_{w_4})$. Solving (32) similarly to (12) yields:

$$P^{(1)}_{e,\text{index}}(h^{(1)}_{1,a_1}) = \mathrm{Q}\left(|U_4|/\sqrt{2}\sigma_n\right), \tag{33}$$

where U_4 is simplified with mean $\mu_{u_4} = 0$ and variance $\sigma^2_{u_4} = (\beta(1+\alpha) + (1-\beta)(\alpha+(1-\alpha)\kappa))\sigma^2_{h^{(1)}}$, implying that $U_4 \sim \mathcal{N}(\mu_{u_4}, \sigma^2_{u_4})$. Averaging (33) as in (13), the near user's average active antenna index error probability is:

$$P^{(1)}_{e,\text{index}} = \frac{1}{2}\left(1 - a/\sqrt{a^2 + 2/\sigma^2_{u_4}}\right). \tag{34}$$

Remark 4: At high SNR, the average antenna index error probability for the near user can be approximated as:

$$P^{(1)}_{e,\text{index}} \approx 1/2a^2\sigma^2_{u_4}. \tag{35}$$

The overall BER for the near user, $P^{(1)}_e$, includes errors from both symbol and active antenna index estimations, given by:

$$P^{(1)}_e = P^{(1)}_{e,\text{index}} + P^{(1)}_{e,\text{symbol}} - P^{(1)}_{e,\text{index}}P^{(1)}_{e,\text{symbol}}. \tag{36}$$

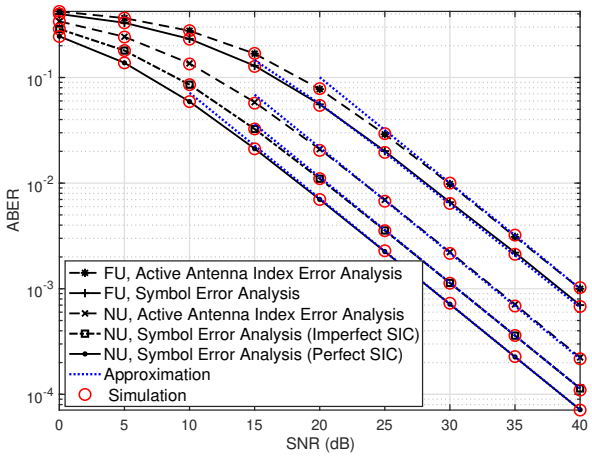

Fig. 3. ABER and Average index error versus SNR for both users.

E. Power Factor Optimization

The ABER of the proposed GSM-NOMA scheme depends on the power allocation factors α and β. The overall ABER at high SNR, denoted as $P_e(\alpha,\beta)$, is computed as the average ABER of the near user $P^{(1)}_e$ and far user $P^{(2)}_e$, given by:

$$P_e(\alpha,\beta) = \frac{1}{4a^2}\sum_{i=1}^{4}\frac{1}{\sigma^2_{u_i}} - \frac{1}{8a^4}\left(\frac{1}{\sigma^2_{u_1}\sigma^2_{u_2}} + \frac{1}{\sigma^2_{u_3}\sigma^2_{u_4}}\right), \tag{37}$$

where $\sigma^2_{u_i}$ is dependent on α and β, representing the channel variance. Optimizing α and β is essential for minimizing ABER while ensuring a balanced power distribution. The optimization problem is formulated as follows:

$$\alpha_0, \beta_0 = \arg\min_{\substack{0\le\alpha\le1\\0\le\beta\le1}} P_e(\alpha,\beta), \tag{38}$$

where the constraints ensure feasible and stable power allocation. Numerical optimization techniques iteratively refine α and β to achieve the optimal values α_0 and β_0, minimizing ABER while maintaining fairness between users.

IV. Results and Discussions

In this section, we solidify the theoretical framework presented in the preceding sections by rigorously validating it with the help of simulations. For clarity and consistency, unless otherwise specified, the simulation environments are defined with the following parameters: $\delta = 2$, and $\sigma^2 = 1$.

Fig. 3 shows the ABER and average index error versus SNR for the near ($d^{(1)} = 1$) and far ($d^{(2)} = 2$) users. Both analytical and simulation results are presented, showing a close match across the SNR range. Notably, the analytical approximations align well with the simulation results at high SNR, validating the accuracy of the derived expressions. The near user consistently outperforms the far user due to better signal quality. Active antenna index errors degrade performance by complicating antenna detection in the absence of modulation schemes. Imperfect SIC impacts the near user's performance by introducing residual interference and reducing detection accuracy, although this gap narrows at higher SNR values.

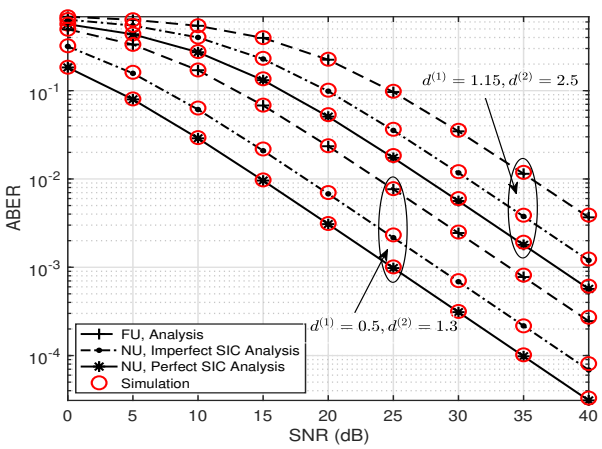

Fig. 4. ABER versus SNR for both users for different $d^{(1)}$ and $d^{(2)}$.

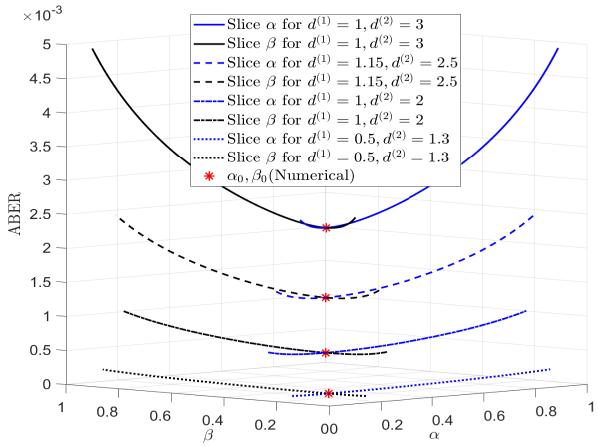

Fig. 5. ABER versus power factors α and β for both users.

Symbol detection benefits from modulation and diversity, leading to improved performance, whereas active antenna index errors and imperfect SIC contribute to degraded outcomes.

Fig. 4 shows simulated and analytical ABER versus SNR for near and far users at varying distances, under both perfect and imperfect SIC. The results closely match, validating the theoretical model. ABER improves with SNR, with the near user consistently outperforming the far user due to proximity and SIC gains. Perfect SIC enables better interference cancellation, while imperfect SIC introduces residual interference, degrading near-user performance. Higher ABER for the far user results from lower SNR and increased path loss. These findings underscore the importance of efficient SIC and resource management in GSM-NOMA systems.

Fig. 5 presents the analytical ABER of the GSM-NOMA scheme versus power allocation parameters α and β at 30 dB SNR for different user distances. The 3D plot shows ABER rising symmetrically as either parameter moves away from its optimum, highlighting the robustness of the optimization. Optimal values (α_0, β_0) vary with user distance: they are symmetric when users are nearby and asymmetric with greater distance gaps, reflecting adaptive power control. Numerical results validate the model, confirming the strategy's effectiveness in minimizing ABER and boosting performance.

V. Conclusion

This paper introduces a novel GSM-NOMA and spatial NOMA framework to enhance spectral efficiency, error performance, and interference resilience in wireless systems. Analytical ABER expressions for both symbol and antenna index detection under perfect and imperfect SIC were derived and validated through simulations. Optimized power allocation factors (α_0, β_0) led to notable ABER reduction. Near users saw improved performance due to better channels, while imperfect SIC caused residual interference at low SNR. Overall, the proposed framework enables efficient resource utilization, robust performance, and adaptability for next-generation wireless networks.

References

[1] B. Patnaik, A. Agarwal, S. Mali, G. Misra, and K. Agarwal, "A review on non-orthogonal multiple access technique for emerging 5G networks and beyond," in *Proc. IEEE Int. Conf. Smart Electron. Commun.(ICOSEC)*, Oct. 2020, pp. 698–703.

[2] F. Boccardi, R. W. Heath, A. Lozano, T. L. Marzetta, and P. Popovski, "Five disruptive technology directions for 5G," *IEEE Commun. Mag.*, vol. 52, no. 2, pp. 74–80, Feb. 2014.

[3] L. Dai, B. Wang, Y. Yuan, S. Han, I. Chih-Lin, and Z. Wang, "Non-orthogonal multiple access for 5G: Solutions, challenges, opportunities, and future research trends," *IEEE Commun. Mag.*, vol. 53, no. 9, pp. 74–81, Sep. 2015.

[4] K. Higuchi and A. Benjebbour, "Non-orthogonal multiple access (NOMA) with successive interference cancellation for future radio access," *IEICE Trans. Commun.*, vol. E98-B, no. 3, pp. 403–414, Mar. 2015.

[5] S. R. Islam, N. Avazov, O. A. Dobre, and K.-S. Kwak, "Power-domain non-orthogonal multiple access (NOMA) in 5G systems: Potentials and challenges," *IEEE Commun. Surveys Tutorials*, vol. 19, no. 2, pp. 721–742, 2nd Quart. 2017.

[6] W. Shin, M. Vaezi, B. Lee, D. J. Love, J. Lee, and H. V. Poor, "Non-orthogonal multiple access in multi-cell networks: Theory, performance, and practical challenges," *IEEE Commun. Mag.*, vol. 55, no. 10, pp. 176–183, Oct. 2017.

[7] R. Y. Mesleh, H. Haas, S. Sinanovic, C. W. Ahn, and S. Yun, "Spatial modulation," *IEEE Trans. Veh. Technol.*, vol. 57, no. 4, pp. 2228–2241, Jul. 2008.

[8] V. Tarokh, N. Seshadri, and A. R. Calderbank, "Space-time codes for high data rate wireless communication: Performance criterion and code construction," vol. 44, no. 2, pp. 744–765, Mar. 1998.

[9] S. P. Singh and P. M. Pradhan, "Effects of imperfect CSI and imperfect SIC on artificial noise assisted precoded multiuser secure NOMA-GSM," in *2023 IEEE ANTS*, Mar. 2023, pp. 491–496.

[10] Y. Liu, L. Xiang, L.-L. Yang, and L. Hanzo, "Space-time coded generalized spatial modulation for sparse code division multiple access," *IEEE Trans. Wirel. Commun.*, vol. 20, no. 8, pp. 5359–5372, Mar. 2021.

[11] T. V. Vinh, P. T. Hiep, and N. T. Phuong, "Combined variable active antenna spatial modulation and NOMA to enhance spectral efficiency for multiple users MIMO systems," in *2022 IEEE ATC*, Nov. 2022, pp. 29–34.

[12] Y. Liu, L.-L. Yang, and L. Hanzo, "Sparse space-time-frequency-domain spreading for large-scale non-orthogonal multiple access," *IEEE Trans. Veh. Technol.*, vol. 69, no. 10, pp. 12 327–12 332, Jul. 2020.

[13] S. Kumar and M. R. Bhatnagar, "Differential modulation-based non-orthogonal multiple access," in *Proc. 2024 IEEE Wireless Commun. Netw. Conf. (WCNC)*, Apr. 2024, pp. 1–6.